UNMANNED SYSTEMS PAPER

Improving Endurance and Range of a UGV with Gimballed Landing Platform for Launching Small Unmanned Helicopters

S. Ioannou · K. Dalamagkidis · K. P. Valavanis · E. K. Stefanakos

Abstract Design specifications for a high-endurance and range unmanned ground vehicle (UGV) with a gimballed landing platform on top of it for takeoff/landing, transporting to the target area and recharging of small/miniature unmanned helicopters are presented and justified. Specification constraints include UGV strict payload limitations, limited free space affecting power supply availability that impacts on-board available energy, limited endurance and operational range, as well as limitations and restrictions related to electric and non-electric small unmanned vertical takeoff and landing (VTOL) vehicles, similar to those of UGV with the most important being limited flying time. Focusing on the All Terrain Robot Vehicle (ATRV-Jr) UGV and a helicopter of the size of the Maxi Joker 2 as a testbed, a detailed analysis of component power consumption reveals reasons for reduced runtime and operational range. After a comparative study of state of the art power supply and battery technologies, a hybrid battery configuration is proposed that improves more than 500% the manufacturer-specified ATRV-Jr endurance (or 1,000% the currently used custom-made ATRV-Jr endurance) by considering: (1) optimum

S. Ioannou (✉) · E. K. Stefanakos
Clean Energy Research Center, Electrical Engineering Department,
University of South Florida, 4202 East Fowler Avenue, ENB 118,
Tampa, FL 33620, USA
e-mail: ioannou@mail.usf.edu

E. K. Stefanakos
e-mail: cerc@eng.usf.edu

K. Dalamagkidis · K. P. Valavanis
Unmanned Systems Lab, Computer Science
and Engineering Department, University of South Florida,
Tampa, FL 33620, USA

K. P. Valavanis
e-mail: kvalavan@cse.usf.edu

design with weight, volume, runtime and rechargeability being major restrictions and concerns, and (2) use of lower power sensors and processors without affecting UGV functionality and operability. A sun-tracking solar array that collects and stores energy is integrated with the UGV gimballed landing platform. Simulations demonstrate the validity of the design. Although the testbed is specific, the design itself is generic enough and suitable for other UGV/VTOL vehicles.

Keywords Endurance improvement · Solar power · Fuel cells · Lithium batteries · Landing platform UGV · VTOL vehicle

1 Introduction

The quest for enhanced autonomy of unmanned vehicles, coupled with the complexity of the missions they are being used for, on one hand, and operational restrictions due to low payload capabilities and small battery capacities, on the other hand, justify the need for novel solutions that improve unmanned vehicle endurance and range without adversely affecting their autonomy and functionality.

Unmanned aerial vehicles are widely used due to their ability to cover large areas and reach points not easily approachable by conventional ground vehicles [10]. As a consequence, runtime limitations of such systems are very important. In particular, small man portable unmanned VTOL vehicles, electric or not, although capable of taking off and landing anywhere, with the ability to hover over areas of interest, suffer tremendously from limited flying times that seldom exceed 30 min. This restricts the operational range, admissible mission profiles and on-board sensors and processors.

Unmanned ground vehicle and unmanned aerial vehicle (UAV) power requirements are mostly determined by the manufacturer for a specific vehicle configuration, ignoring the impact of possible upgrades, off-the-self add-on sensors and other custom made accessories, such as multiple cameras, inertial measurement unit (IMU), global positioning system (GPS), compass, laser range finders and sonar sensors in addition to computer-controlled servos, navigation systems, and cooling fans. For UAVs, in addition to the above, the very low payload capabilities offer no room for major improvements.

Therefore, it is the central objective of this paper to overcome said limitations by presenting specifications for an integrated UGV-gimballed landing platform–unmanned VTOL vehicle system with optimal power consumption and low-power sensors that improve the UGV endurance by more than 500% and, indirectly, increasing the VTOL vehicle operational range as the VTOL vehicle is transported to the mission site without the need to fly. The proposed gimballed platform, which will be a power source itself, rotates around two axes perpendicular to each other, allowing the VTOL to take off and land, regardless of the position of the UGV, while securing it during transportation.

The idea of landing a VTOL vehicle on a mobile platform is not new. The problem of autonomously landing a full-size helicopter on a ship has already been investigated in [27]; it is a dangerous and difficult problem to solve even for manned helicopters with experienced crews. However, this topic has not been researched for miniature VTOL vehicles. In fact, a literature search has revealed only one design for

autonomous launching, retrieval, and refueling of UAVs, developed by SPAWAR Systems Center and Allied Aerospace as part of the Autonomous UAV Mission System (AUMS) project [20]. An initial demonstration of the capabilities of this system was done in 2003. This system was specifically designed to be used with Allied Aerospace's iSTAR UAV and SSC San Diego's MDARS UGV. However, adaptation to other systems is not possible, as compared to the design presented in this paper.

A detailed analysis is carried out for an ATRV-Jr UGV with custom-made components and a gimballed landing platform suitable for small VTOL vehicles like the Raptor 90 or the Maxi Joker 2. However, the same analysis/design may be followed for any UGV/VTOL combination. Requirements for energy storage devices are set for 10 h of continuous operation under maximum load (as compared with the 1 h of the currently used custom made mobile platform) and two recharges of an electric unmanned VTOL. As improved endurance is of the highest priority set, requirements are coupled with recommendations for very low power efficient sensors that do not limit functionality and flexibility. Before proceeding, it must be stated that it is beyond the scope of this paper to study how the VTOL will take off/land autonomously or how it will be controlled.

The contributions of this paper, major and minor, are manifold: the first is a complete comparative study of available power sources and battery technologies for UGVs that clarify reasons for reduced endurance; the second is a step-by-step thorough analysis of UGV component power requirements followed by recommendations for the use of low power sensors that do not affect vehicle functionality; the third contribution is the design specifications for an order of magnitude higher endurance UGV compared with the existing one, based on a hybrid battery configuration; a fourth contribution is the design itself of an energy-efficient (solar cell) gimballed landing platform serving as a transport and recharging base for small unmanned helicopters. An indirect benefit of this design is that it also allows the VTOL vehicle to take off from one UGV and land on another, maximizing operational range.

The rest of the paper is organized as follows. The state-of-the-art in power systems and types of batteries is presented, followed by the characteristics of the UGV and VTOL under investigation. After that, current power requirements of the UGV are summarized, followed by the design of the landing platform and the derivation of all necessary equations for its operation. Several alternatives for improvement of the ATRV-Jr endurance are investigated, followed by a description and the advantages of installing a solar array on the landing platform.

2 State-of-the-Art in Battery Technologies

Current UGV power sources are almost exclusively rechargeable lead acid and nickel cadmium (NiCad) batteries due to the fact that both technologies are mature, well understood and cheaper compared to more recent technologies such as lithium batteries and fuel cells.

Recent concerns about energy and environmental problems and advances in material and manufacturing engineering have enabled a wider commercial product selection in lithium batteries and fuel cells. For example, proton exchange membrane

fuel cells (PEMFCs) have already been tested and used in Autonomous Underwater Vehicles (AUVs) [22, 23, 29, 31] and mobile robots [15, 30]. As stated in [23], direct methanol fuel cells (DMFC) are a better choice for mobile robots, but wide power range units are only in the first steps of their commercialization.

New generation VTOLs, such as the Raptor 90, use a gas motor and batteries such as NiCd and Lithium Polymer (LiPo) for the servos and computer. In like manner, electric VTOLs, such as the Maxi Joker 2, use NiMH and NiCad batteries with runtime of 5–12 min for 28–32 cells (5.2–5.5 kg), whereas 10–12 cells (4.5–5 kg) of LiPo can increase the runtime to 8–20 min. respectively.

2.1 Batteries

Battery technology profiles are summarized in Table 1, with NiCad being the oldest technology. Its high life cycle, low internal resistance, and high load current characteristics make it an attractive choice for power tools, two-way radios, and biomedical instruments. Reusable alkaline batteries, on the other hand, are very cheap, but their high internal resistance limits their use to only very low current applications. Furthermore, despite low energy density, low price makes sealed lead acid (SLA) batteries attractive for applications where volume and weight is not a problem. Lithium ion batteries are the most expensive. With high energy density and cell voltage, lithium technology is an attractive choice for electronic devices where dimensions and weight are critical, such as consumer electronics. Furthermore, material technology advancements have enabled manufacturing of scaled up lithium batteries for satellite and electric vehicle applications.

2.2 Fuel Cells

Secondary batteries have limited runtime that is directly proportional to energy density and inversely proportional to load characteristics, with the recharging process requiring several hours. On the other hand, fuel cells are capable of providing power for as long as fuel (usually hydrogen) is available.

Furthermore, the refueling process can take less than a few minutes, which presents a significant improvement over the hours usually required for recharging of batteries.

Table 1 Battery technology profile [2, 3]

	NiCd	NiMH	SLA	Li-Ion	Reusable alkaline
Energy density (Wh/Kg)	40–60	60–80	30	165	80 (initial)
Internal resistance (mΩ)	100–300	200–800	< 100	300–500	200–2000
Cycle life	1500	500	200–300	500–1000	10000
Cell voltage	1.2	1.2	2	3.6	1.5
Load current	> 2C	0.5–1C	0.2C	2C	0.2C
Operating temperature (°C)	−40 to +60	−20 to +60	−20 to +60	−20 to +60	0 to 65
Cost	$50	$70	$25	$100	$5
In commercial use since	1950	1990	1970	1991	1992

Table 2 Fuel cell technology profile [5]

	PAFC	AFC	MCFC	SOFC	SPFC	DMFC
Operating temperature (°C)	150–210	60–100	600–700	900–1000	50–100	50–100
Power density (W/ cm^2)	0.2–0.25	0.2–0.3	0.1–0.2	0.24–0.3	0.35–0.6	0.04–0.23
Projected life (h)	40,000	10,000	40,000	40,000	40,000	10,000
Projected cost (US$/KW)	1000	200	1000	1500	200	200

Table 2 summarizes some of the characteristics of the various fuel cell technologies currently available. From these technologies the proton exchange membrane fuel cells (PEMFCs) are the most attractive choice for portable applications because of their low operating temperatures. The primary fuel used in PEMFCs is hydrogen, which entails an added complexity regarding storage and handling [19]. As an alternative a subset of PEMFCs, the direct methanol fuel cells (DMFCs) uses methanol as a fuel. Although in general DMFCs are considered to be less efficient than PEMFCs, they are very attractive for subkilowatt, portable applications. This is due to the fact that they feature high energy densities and use a liquid fuel that, although toxic, is easier to handle.

2.3 Supercapacitors

Batteries and fuel cells have limited power densities that limit fast response to greater-than-average load power demands. This power quality problem may cause the computer to reset and motors to stall. A common solution to this problem is to oversize the battery at the expense of cost, weight and size. Unlike batteries and fuel cells, supercapacitors have very high power but very low energy densities that limit their use as a primary power source. Currently one of the highest reported energy densities of supercapacitors is 8 Wh/kg [16] – too small to practically replace a battery pack. However, a high energy density device (battery) may be connected in parallel to a high-power device (supercapacitor) to form a hybrid power supply combination. Research reported in [4, 6, 9, 17, 18] has shown that a hybrid configuration is a more efficient solution than oversizing a battery.

3 ATRV-Jr and Maxi Joker 2 Specifications: Power Consumption and Endurance

The ATRV-Jr is manufactured by the iRobot Corporation and it has the following characteristics, as specified by the manufacturer [26]:

–   Speed (m/s): 1
–   Height (cm/in): 51/20
–   Length (cm/in): 78/30.7
–   Width (cm/in): 63/24.8
–   Weight (kg/lbs): 50/110
–   Payload (kg/lbs): 25/55
–   Endurance: 3–5 hr (terrain dependent)

The Maxi Joker 2 is a middle-sized, remote-controlled, electric, miniature helicopter. It can be modified to operate as an autonomous system by the incorporation

of a lightweight vision system, a processing system as well as a communications platform. Its characteristics according to the manufacturer are:

–   All-up weight (kg/lbs): 8/17.6
–   Payload (kg/lbs): 2/4.4
–   Endurance: up to 20 min

Based on manufacturer specifications the ATRV-Jr is powered by two lead acid batteries, 12 Kg (27 lbs) and 4 dm^3 (343 in^3) each, with a total capacity of 672 Wh.

Without any upgrades or other additions, only the computer and vehicle motors are connected directly to the batteries. The Pentium 3 800-MHz computer requires 1.25 A at 24 V, whereas the two motors require 5.44 A total (2.72 A each). Taking into account the inefficiencies of the computer power supply and the motors, the full load current is estimated to be 7.5–8 A and as a consequence the runtime is approximately 3.5 h. Terrain dependency, smaller loads like cooling fans and 17 sonar sensors and losses result in runtime variation between 3 and 5 h.

With current upgrades and added sensors, 2 DC/DC converters and a 300-W ATX power supply are connected directly to the batteries to provide regulated voltages to power the sensors and the on-board computer (Fig. 1). The processor was upgraded to a 3-GHz Pentium 4 requiring 120 W. Considering a 70% ATX power supply efficiency (built for desktops) and the power consumption of the other subsystems (storage, communications, etc.) the total computer power consumption is estimated to be 214 W. Total peak sensor power demand is 86 W, increased to 107 W when considering 80% efficiency for the DC/DC converters and voltage regulators. This analysis gives a full load of 452 W and a corresponding current of 18.8 A.

Figure 1 depicts the performance of the battery pack with respect to the discharge current. At a discharge current of 1.65 A, the battery pack has a capacity of 33 Ah or 20 h runtime, whereas at a current of 19.7 A the capacity drops to 19.7 Ah or 1 h of runtime. Therefore, for the previously estimated load current of 18.8 A, the runtime is estimated to be barely more than 1 h. This runtime does not take into account any capacity loss due to aging.

The flight time of the Maxi Joker 2 is determined by the battery pack used and it can go up to 20 min. In the case of the Raptor 90, maximum fly runtime is determined

Fig. 1 Capacity (Ah) and discharge time (Hours) versus discharge current of deep cycle DCS-33H lead acid batteries
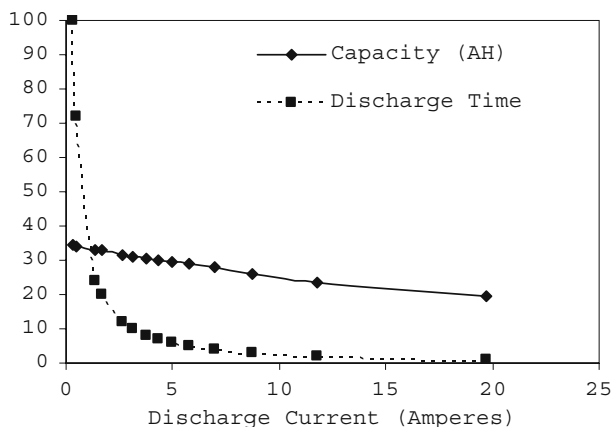
by the amount of available fuel and vision system operation. As shown in [10], available fuel limits maximum runtime to 18 min. The vision system with CPU utilization between 98% and 100% and a wireless connection providing GPS coordinates to an external system, was operated continuously for 35 min. With low power, an efficient vision system already in use, and with payload capability reached, the options for endurance improvements are extremely limited for miniature VTOLs.

4 Increasing VTOL Endurance and Range

It has been already demonstrated that improving the endurance of VTOL vehicles is not possible due to payload limitations, high energy demands, and the power storage technology currently employed. Nevertheless, it is possible to indirectly increase the range of VTOLs by transporting them to the area of interest and using their runtime over the target rather than en route. This is achieved with the installation of a gimbaled landing platform on top of a UGV.

This gimbal-based design has been used extensively, albeit in a relatively smaller scale. The gimbal usually consists of two or three concentric rings that are connected with each other by axes, each of which is driven by an individual motor. As a result, each ring can rotate independently of the other, keeping the inner gimballed platform horizontal and free from vibrations. This is usually achieved with installation of gyros, which calculate the angles of rotation of the platform providing the necessary information to the motors to counter any movement of the gimbal support [14]. Currently, the main application of gimbaled systems is the stabilization of cameras on helicopters.

Gimbaled platforms allow for one, two, or three-axe rotation, but a two-axe gimballed system is sufficient for landing purposes. There is no need to install gyros, as altitude data can be supplied by the IMU of the UGV itself. This design is chosen because it levels the landing pad with no limitation with respect to the pose of the UGV. The cross section of the platform is seen in Fig. 2 and a 3D representation of the platform on top of an ATRV-Jr is depicted in Fig. 3. Platform rotation can be achieved with the use of two motors connected via a geared system to the two rotation axes. The gears will take most of the load off the motors and make the platform more resistant to movement due to weight imbalance. The power requirements of the motors are estimated to be approximately 25W.

5 UGV with Takeoff/Landing Platform: Lower Power Demand, Higher Efficiency, and Endurance

It is true that for most UGV outdoor applications, payload needs sensor suite utilization and, as a consequence, energy requirements are a priori unpredictable.

Fig. 2 Cross-section of a two-axis gimbaled platform design

Elevation

Azimuth
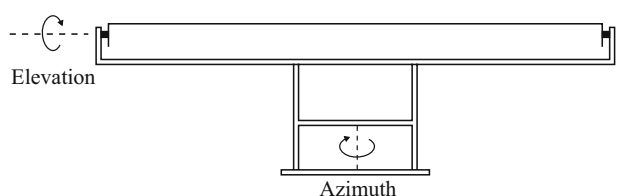
**Fig. 3** 3D representation of the platform installed on top of an ATRV-Jr
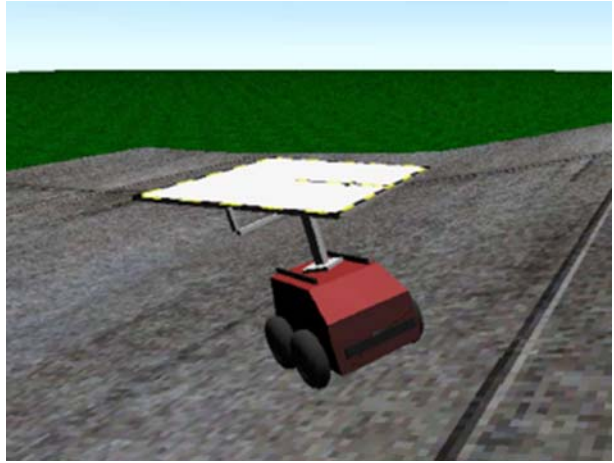
This makes proper sizing of energy storage devices a rather difficult task. However, this research considers a wide range of outdoor applications related to search and rescue, surveillance, mapping, de-mining threat identification, and patrolling and, therefore, the requirements for energy storage devices have been sized for 10 h of continuous operation under maximum load. This also includes the operation of the landing platform and two recharges of an electric unmanned VTOL (Fig. 4). As improved endurance is of high priority, set requirements are coupled with recommendations for more efficient sensors.

5.1 Sensors and Processing Platform

The current configuration of the ATRV-Jr with all sensors and power consumption requirements is presented in Table 3. The cameras alone consume up to 60 W out of the total consumption that is about 85.5 W! As a first step to save energy, lower

Fig. 4 Screenshots every 2 s of a simulated VTOL landing
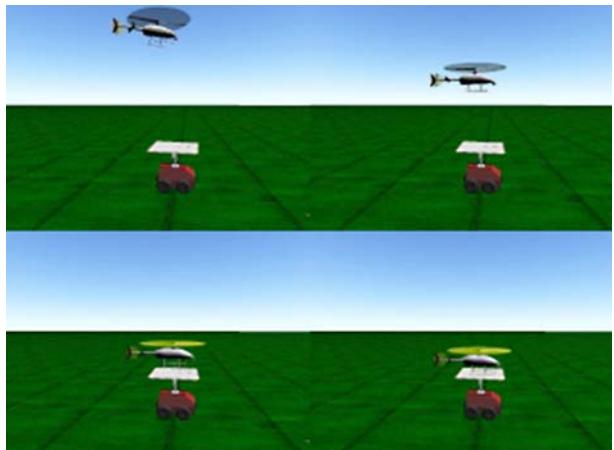
Table 3 ATRV-Jr current sensors

Sensor type	Voltage (V)	Power (W)
Laser	24	17.5
Fans (two)	24	4.1
IMU	12	3
Fan	12	0.2
Sony cameras (two)	12	60
GPS	9	0.6
Compass	5.1	0.1
Total consumption		85.5

power sensors that offer the same capabilities with the existing ones are proposed as shown in Table 4. These sensors consume only 9.3 W, resulting in a significant reduction of 90% and 13% in the sensor and total power consumption, respectively.

The proposed new sensors have been selected with low power consumption in mind. As a result, some of the sensors have limited capabilities compared to the older sensors. However, these limitations do not affect the overall system performance and applications. For example, the older laser (SICK LMS200) has a range of 80 m but consumes 17.5 W, whereas the new proposed one (Hokuyo URG-04LX) has a range of 4 m and consumes only 2.5 W. However, for applications such as collision avoidance at speeds of 1 m/s, the older laser was oversized and unnecessary. The new proposed laser can meet the application at much lower power consumption.

As a second step, a comparative study of processor power consumption (for processors with 3 GHz clock speed) shown in Table 5 has revealed that the Pentium 4 processor with 3 GHz clock speed consumes as much power as the two motors of the ATRV-Jr.

As observed in Table 5, the two Intel processors tested at 3 to 3.4 GHz for maximum work load required 131 and 134 W, respectively [11]. At idle state, Intel speed step technology reduces the power consumption to 50 W by running the processor at 2.865 GHz. On the other hand, the AMD processor at the same clock speeds consumes only 45.6 W under load and 11.6 W in idle mode. Furthermore, the Pentium M processor, specifically designed for mobile applications, has a maximum power consumption of 30 W at 2.66 GHz clock speed, whereas at idle state the demand drops to 21 W by reducing the clock speed to 1.2 GHz.

The recommendation is to use a Pentium M 2.66 GHz and Compact Flash memory for storage. Compact Flash memory has the advantage of low power consumption [32], vibration resistance, and plug in–plug out capability. The latter feature makes

Table 4 Proposed low power sensors

Sensor type	Power (W)
Sony CCTV camera–FCB (2)	6
GPS-Carmin 18, 12 channel	0.3
IMU–ETB	0.5
Range finder HOKUYO URG-04X	2.5
Total consumption	9.3

Table 5 Processor power consumption (from [11–13])	Processor type	Power demand (Watts)	
		Idle state	Max work load
	Intel Pentium D 820	50	134.3
	Intel Pentium 4	49	130.6
	Intel Pentium M	20.8 at 1.2 GHz	30 at 2.66 GHz
	Intel Pentium 0.13 μm	30 at 1.6 GHz	76 at 3.2 GHz
	Intel Pentium 90 nm	30 at 1.866 GHz	88 at 3.33 GHz
	AMD Athlon64, +3500	11.6	45.6

programming of the ATRV-Jr easier and allows for storage of various mission scenarios in different memory modules, loading them as needed.

With the proposed configuration, maximum power demand of the processor including that of the proposed sensors is about 40 W. The use of a high efficiency power supply like the M1-ATX with 80–90% efficiency is proposed, as opposed to the currently used desktop power supply with 60–70% efficiency. As a result, the total estimated power consumption of the sensors and processing platform is reduced from 321 to 50 W only. In summary, After the stated recommendation for low power sensors, processor, and power supply results in a decrease of the total full load power demand (including the motors) by 60% (from 452 to 181 W) and, as a consequence, a runtime increase from 1 to more than 3 h.

5.2 Powering the ATRV-JR with Lithium Batteries

Before determining the energy requirements for accomplishing the runtime goal of 10 h, the consumption due to platform operation and VTOL recharging needs to be estimated. The takeoff/landing platform on top of the UGV has an estimated power consumption of 25 W, which will not be taken into account since it will operate only for a few minutes and therefore its contribution to the total power consumption is minimal. On the other hand, VTOL recharging needs approximately 100 Wh for every recharge. Thus, the total required energy to achieve the set goal is estimated to be 2 kWh resulting in a required battery capacity of 84 Ah.

By comparing the current lead acid with a high energy Li-ion battery pack in Table 6, it is evident that the set goal can be achieved with a significant reduction

Table 6 Comparison of lead acid and Li-Ion battery packs		DCS-33 lead acid	Li-Ion VL45E cells, 7 x 2 matrix, by Saft
	Capacity (Ah)	26 at C/3	90 at C/3
	Voltage (V)	24	25.2
	Weight (Kg)	24	15
	Total energy (Wh)	624	2268
	Specific energy (Wh/Kg)	26	151
	Energy density (Wh/dm^3)	78.6	318
	Specific power (W/Kg)	208	664
[1] Under maximum load	Power density (W/dm^3)	604	1392
[2] For a mixed cycle of 30% stationary and 70% moving operation	Worst case runtime[1] (hr)	3.2	11
	Average runtime[2] (h)	4.2	14

in the on-board battery weight. Specifically, a decrease of more than 37% (from 24 to 15 kg) is possible, which will allow an equivalent increase in the payload capacity of the system.

However, lithium batteries may not be the best available choice; current commercial scale-up lithium batteries require at least 2 to 3 h to charge. For this reason, fuel cells offer a better choice for powering the ATRV due to their easy refueling process. This recommendation is justifiable since, as stated in [31], the Urashima AUV had an increase in travel distance of 65.4% when powered by a fuel cell system instead of lithium ion batteries.

5.3 Using a Combination of Lithium Batteries and a Fuel Cell

As most commercially available DMFCs do not meet the required power demand, an alternative approach is to combine a system like the 250-W iGen system, provided by Idatech, with Li ion cells. This hybrid system's capacity depends on the on-board fuel storage. Table 7 shows the characteristics of the hybrid system for 2.5 and 7.5 kg of fuel for a total system weight between 19 and 24 kg (the latter being equal to the currently installed battery pack.

Finally, the high energy density DMFC and high power density Li-ion design can be classified as a hybrid system similar to battery and supercapacitor hybrid systems. An active hybrid system is proposed instead of a passive hybrid system. The introduction of a control system, DC/DC converter [7], eliminates all the negative effects of a passive hybrid system and gives more design flexibility. Furthermore, it has been shown that a multilevel DC/DC converter can provide optimum fuel cell utilization [21].

5.4 Using a Solar Array

In order for the VTOL to safely perform an autonomous vision-based landing, significant margins of error need be accommodated and therefore the actual area of the landing platform is chosen to be 1 m^2, which is four times that of the footprint of the Maxi Joker 2. This free level surface can be covered with a photovoltaic array.

Table 7 Alternative solution (DMFC AND BATTERY)

	iGen DMFC by Idatech	Li-Ion VL45E cells, 7 x 1 matrix, by saft	Total performance
Capacity (Ah)	56.3–168.8	45	101.3–213.8
Voltage (V)	24	25.2	24
Weight (kg)	Unit 9.0 kg Fuel 2.5–7.5 kg	7.5	19–24
Total Energy (Wh)	1,351–4,050	1,134	2,485–5,184
Specific Energy (Wh/kg)	117.5–245.5	151.2	130.8–216
Specific Power (W/kg)	21.7–15.2	664	275.2–218
Worst case runtime[1] (h)	–	–	12.4–26
Average runtime[2] (h)	–	–	15.4–32

[1]Under maximum load

[2] For a mixed cycle of 30% stationary and 70% moving operation

Although a portion of the array will be shaded by the VTOL, it is estimated that about 50 to 70% will receive solar radiation at all times. The total area available on the landing platform is then used to provide up to 120 W of energy under ideal conditions. Even with a more realistic performance of 50 to 60 W, it is still adequate to cover the needs of the sensors and the on-board computer. As a result, while the UGV is stationary it will not consume battery power, and consequently its endurance will increase significantly.

Furthermore, when the VTOL is air-born the available rotation mechanism of the platform can be used to align the solar array with the sun, thus maximizing the former's performance and allowing battery recharging to take place. The energy output of the solar array was not taken into account into the sizing of the lithium battery pack and the fuel cell. This is because in the worst case, for example a rainy day, the solar array's contribution will be negligible. On the other hand, on an average sunny day and during a 10-h mission, the solar array can produce up to 500 Wh, which is 25% of the total energy demand.

Even in the case where the motors of the rotation platform mechanism are assumed to be active at all times, then for a 10-h operation, a 250-Wh power consumption would be required. In this case, the photovoltaic array would cover this amount plus 12.5% of total mission energy demand, thus extending runtime even more. Therefore, a conservative design and estimation is proposed.

6 Leveling the Platform

To derive the equations needed to level the platform, an orthogonal Cartesian system in 3D space is used, where the x axis is horizontal, the y axis is vertical, toward the sky, and the z-axis is toward the viewer (Fig. 5a). Using a matrix notation to represent the rotations of any object we have the following [1, 8]:

$$\mathbf{R}\left(\phi\right)=\begin{bmatrix} 1 & 1 & 0 \\ 0 & \cos\phi & -\sin\phi \\ 0 & \sin\phi & \cos\phi \end{bmatrix} \tag{1}$$

$$\mathbf{P}\left(\phi\right)=\begin{bmatrix} \cos\phi & -\sin\phi & 0 \\ \sin\phi & \cos\phi & 0 \\ 0 & 0 & 1 \end{bmatrix} \tag{2}$$

$$\mathbf{Y}\left(\phi\right)=\begin{bmatrix} \cos\phi & 0 & \sin\phi \\ 0 & 1 & 0 \\ -\sin\phi & 0 & \cos\phi \end{bmatrix} \tag{3}$$

where $\mathbf{R}$ is the roll matrix, $\mathbf{P}$ is the pitch matrix, and $\mathbf{Y}$ is the yaw matrix. The roll, pitch, and yaw angles are defined by a rotation around the z, x and y axes, respectively (Fig. 5b–d). Any rotated vector V can be calculated by a combination of the rotations mentioned above using the formula below:

$$V' = \mathbf{R}\left(\phi_1\right).\mathbf{P}\left(\phi_2\right).\mathbf{Y}\left(\phi_3\right).\mathbf{V}, \tag{4}$$

where the sequence with which each operation is applied is important.

Fig. 5 (**a**) The Cartesian system used. (**b–d**) Graph b shows a vector located on the *y–z* surface being rotated around the *x*-axis. The angle corresponds to the roll of the vector. In like manner, graphs c and d show rotations around the *y* and *z* axes, respectively, that correspond to a change in yaw and pitch
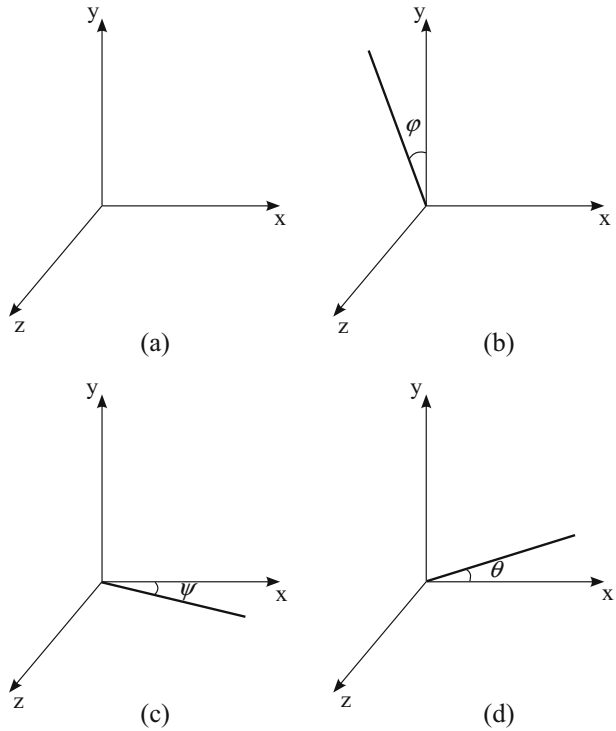
Assuming that during its movement the robot reached a position where its roll, pitch, and yaw angles are ϕ_1, ϕ_2, ϕ_3, respectively, then it follows that as a consequence the platform as well, has the same roll, pitch, and yaw with respect to the horizontal. The landing platform is designed with the capability of rotating around two axes (Fig. 6), a vertical one and a horizontal one, which henceforth will be referred to as the azimuth axis and the elevation axis, respectively. To level the platform, suitable ϕ_4, ϕ_5 angles for the azimuth and elevation vectors, respectively, need to be calculated.

The problem can be divided into two subproblems where the platform is first rotated around the azimuth axis until the elevation axis is horizontal. Then by rotating around the elevation axis until the azimuth axis is vertical, the platform assumes a horizontal pose. The initial elevation vector is given by:

$$V_{el} = \mathbf{R}(\phi_1).\mathbf{P}(\phi_2).\mathbf{Y}(\phi_3).\mathbf{V}_z \tag{5}$$

where V_z is the *z*-axis unitary vector and is equal to [0 0 1].

After the platform has been rotated around the azimuth vector, the new elevation vector becomes:

$$V'_{el} = \mathbf{Y}(\phi_4).\mathbf{V}_{el} \tag{6}$$

Fig. 6 The landing platform
rotates around two axes, a
vertical (azimuth) and a
horizontal (elevation). These
two axes are defined by the
azimuth and elevation vectors
depicted above. Using these
two axes it is possible to
achieve any platform
orientation desired
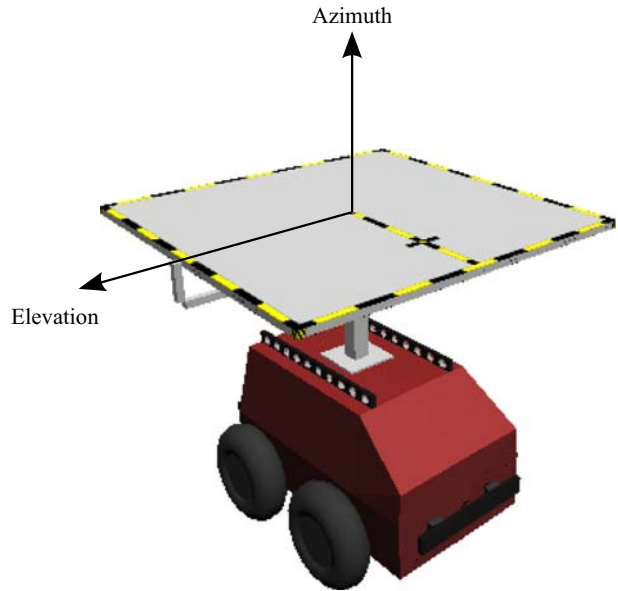
as a change of the azimuth corresponds to a change of the yaw of the platform. Since
the elevation axis needs to be horizontal, the dot product of the elevation vector and
the y-axis is set to zero and the ϕ_4 angle is calculated.

$$V'_{\text{el}} \bullet V_y = 0 \Rightarrow \phi_4 = \tan^{-1}\left(\frac{\cos\phi_2 . \sin\phi_1}{\sin\phi_2}\right) \tag{7}$$

where V_y is the y-axis unitary vector and is equal to [0 1 0].

After the azimuth has been changed, the platform will be rotated around its new
elevation vector, until the azimuth vector is vertical. The azimuth vector before this
rotation is

$$V_{\text{az}} = \mathbf{R}(\phi_1) . \mathbf{P}(\phi_2) . \mathbf{Y}(\phi_3) . \mathbf{Y}(\phi_4) . V_y \tag{8}$$

Since the rotation above corresponds to a change of pitch for the platform, it will
become:

$$V'_{\text{az}} = \mathbf{P}(\phi_5) . V_{\text{az}} \tag{9}$$

The angle ϕ_5 is calculated so that the V_{az} vector will be vertical by setting its dot
product with either the x-axis or the z-axis to zero.

$$V'_{\text{az}} \bullet V_{\text{x}} = 0 \Rightarrow \phi_5 = \tan^{-1}\left(\frac{\sin\phi_2 - \tan\phi_3 . \tan\phi_1}{\tan\phi_3 . \sin\phi_4 - \cos\phi_1 . \cos\phi_2 . \cos\phi_4}\right) \tag{10}$$

where V_x is the x-axis unitary vector.

7 Alignment of Solar Array with the Sun

The alignment of the solar array with the sun to maximize its performance is achieved using the methodology of the previous section. To start with, the sun vector V_{sun} is calculated as the normalized vector with its origin the center of the platform and its destination the sun.

The calculation of the ϕ_4, ϕ_5 angles for azimuth and elevation respectively is done like in the previous section; in two steps. First, the azimuth vector is changed until the elevation vector V_{el} is vertical to V_{sun}. Then the platform is rotated around the axis defined by the elevation vector until the azimuth vector V_{az} is parallel to V_{sun}. The following two equations can be used to determine the final ϕ_4, ϕ_5 angles.

$$V_{\text{sun}} \bullet [\mathbf{R}(\phi_1) \cdot \mathbf{P}(\phi_2) \cdot \mathbf{Y}(\phi_3) \cdot \mathbf{Y}(\phi_4) \cdot \mathbf{V}_z] = 0 \tag{11}$$

$$V_{\text{az}} = \mathbf{R}(\phi_1) \cdot \mathbf{P}(\phi_2) \cdot \mathbf{Y}(\phi_3) \cdot \mathbf{Y}(\phi_4) \cdot \mathbf{P}(\phi_5) \cdot \mathbf{V}_y \tag{12}$$

$$V_{\text{sun}} = \frac{V_{\text{az}}}{|V_{\text{az}}|} \tag{13}$$

In order for the V_{sun} vector to be calculated, it is possible to use geographical data from the region of operation of the system in combination with chronological data (day of year and time of day). Alternatively active sun-tracking methods can also be employed using a vision system or other special purpose equipment, although that would further decrease the payload capabilities of the platform.
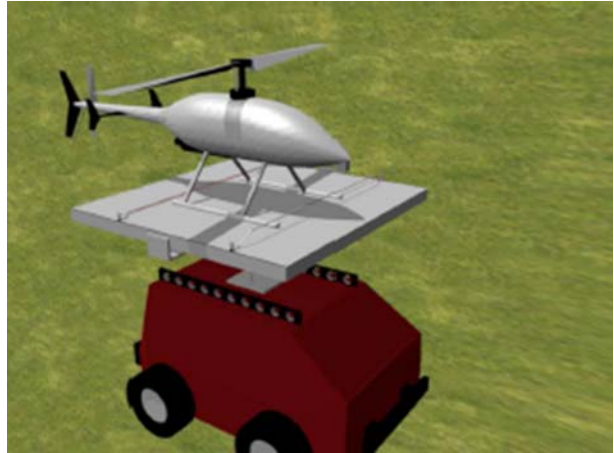
8 Simulation Results

To demonstrate the feasibility of the design, simulations of the robotic platform equipped with a landing platform were carried out, using the Gazebo 0.5.3 (cvs121305) software [25]. This software is open source and is part of the Player/Stage/Gazebo software package. The object dynamics are calculated using the Open Dynamics Engine by Russel Smith [24], which is also used by several simulation applications as well as games.

The landing platform was simulated as a solid mass weighing 12 kg and the moving understructure was modeled using several smaller geometries with a total mass of 3.2 kg. The modeled weight of the platform corresponds to the weight of two readily available commercial solar panels, with an area equal to that of the platform and a total rated output of 120 W (Sunwize SW60, [28]). Two motors are used to move the platform at low speeds. The elevation motor has a stop at $\pm 40°$, while the heading motor is limited to $\pm 90°$. The controller instructs the motors to rotate the platform until the deviation from the predetermined angle is within $\pm 1.7°$.

In all test scenarios, it was possible to rotate the platform until it was horizontal within the predetermined limits of error using only two axes of rotation. Further testing indicated that under the assumption of small and slow changes in the robot pose (roll, pitch and yaw), it is possible to control the platform so that it will remain horizontal while the robot was moving, without significant increase in the error.

Finally, simulations also demonstrated that the installation of the platform resulted in moving the center of gravity of the robot higher, thus making it unstable in higher degrees of inclination.

A concept video demonstrating an unmanned helicopter landing as well as the operation of the securing mechanism (Fig. 7) can be found in the home page of the Unmanned Systems Lab (http://www.cse.usf.edu/USL/Videos/latch-pdemo.mpeg). A second video demonstrates how multiple platforms can be used for border patrol (http://www.cse.usf.edu/USL/Videos/patrol.mpg).

9 Conclusions

This paper examined and identified reasons for the reduced UGV endurance, and, in particular, of a custom-made ATRV-Jr. As presented, the reasons were not only limited to the use of the inefficient lead acid batteries but also included an excessive power demand that exponentially decreased the battery discharge time. To achieve longer runtimes, it is recommended first to use lower power and more efficient sensors rather than oversizing the battery packs. Low-power sensors, a Pentium mobile processor, and a 90% efficient power supply may decrease power consumption by 60%. It has been shown that lithium ion technology meets the set energy requirements of the 10-h goal with only 15 kg, whereas lead acid technology would require more than 72 kg. On the other hand, a combination of a DMFC and Li ion can achieve very high energy densities that can offer runtimes of more than 24 h. The proposed DMFC and Li-ion solution also offers a refueling time of just a few minutes, whereas Li-ion batteries need several hours. Therefore, for outdoor applications such as search and rescue, DMFC combined with Li-ion cells is the most suitable design considering refueling time, weight, volume, and runtime.

It was also demonstrated that although increasing the endurance of modern miniature VTOL vehicles is not possible, it is possible to increase their operational range using a mobile landing platform. In addition, the landing platform provides the opportunity for on-site energy production from renewable energy sources, thus further increasing the VTOL's as well as the UGV's endurance.

References

1. Baker, M.: Euclidean space. http://www.euclideanspace.com/ (2005)
2. Buchmann, I.: Understanding your batteries in a portable world. Article on battery choice and maximize service life. In: Proc. of the Fourteenth Annual Battery Conference on Applications and Advances, pp. 369–373 (1999)
3. Buchmann, I.: Batteries in Portable World, 2nd edn. Cadex Electronics Inc, Canada (2001)
4. Bullard, G.L., Sierra-Alcazar, H.B., Lee, H.L., Morris, J.L.: Operating principles of the ultracapacitor. IEEE Trans. Magnetics. **25**(1), 102–106 (1989)
5. Chan, C.C.: The state of the art of electric vehicles. J. Asian Elect. Veh. **2**(2), 579–600 (2004)
6. Conway, B.E.: Electrochemical supercapacitors: Scientific Fundamentals and Technological Applications, 1st edn. Springer, New York (1999)
7. Dougal, R.A., White, R.E.: Power and life extension of battery-ultracapacitor hybrids. IEEE Trans. Compon. Packag. Technol. **25**(1), 120–131 (2002)
8. Dunn, F.: 3D Math primer for graphics and game development. Wordware, Texas, USA (2002)
9. EPCOS, Electronic Parts and Components (2005) General technical information ultracapacitor technology. www.epcos.com/ultracapacitor.htm
10. Garcia, R., Valavanis, K., Kontitsis, M.: A high power, inexpensive on-board vision system for miniature unmanned VTOL vehicles. Tech. Rep. 4, CRASAR, USF (2005)
11. Gavrichenkov, I.: CPU Category – Intel Pentium D 820 CPU Review, Page 3, 05/27/2005. http://www.xbitlabs.com/articles/cpu/display/pentiumd-820_3.html (2006)
12. Intel United States: Mobile Intel Pentium 4 ProcessorsM, Enhanced Intel SpeedStep Technology. http://www.intel.com/support/processors/mobile/pentium4/sb/cs-007499.htm (2006)
13. Intel United States: Mobile Intel Pentium 4 ProcessorsM, Voltage Requirements. http://www.intel.com/support/processors/mobile/pentium4/sb/cs-007501.htm (2006)
14. King, A.D.: Inertial navigation-40 years of evolution. GEC Rev. **13**(3), 140–149 (2003)
15. Laboratories, S.N.: Robotics online – fuel cell powered mobile robots case study. http://www.roboticsonline.com/public/articles/index.cfm?cat=99 (2006)
16. Latt, M., Leis, J., Arulepp, M., Kuura, H., Lust, E.: Latest developments in carbide derived carbon for energy storage applications. In: Proc. of 16th International Seminar on Double Layer Capacitors and Hybrid Energy Storage Devices (2006)
17. Mastragostino, M.: Electrochemical Supercapacitors in Advances in Lithium Ion Batteries chap. 16. Kluwer Academic/Plenum (2002)
18. Maxwell Technologies: Ultracapacitor application notes. www.maxwell.com/ultracapacitors/support/app_notes.html (2005)
19. Meng, N.: Feasibility study of renewable hydrogen in Hong Kong. Research Seminar on Thermofluid Mechanics (2004)
20. Mullens, K., Pacis, E., Stancliff, S., Burmeister, A., Denewiler, T., Bruch, M., Everett, H.: An automated UAV mission system. In: AUVSI Unmanned Systems in International Security, SPAWAR Systems Center, Allied Aerospace (2003)
21. Ozpineci, B., Tolbert, L.M., Su, G., Du, Z.: Optimum fuel cell utilization with multilevel DC-DC converters. In: Proc. of Nineteenth Annual IEEE Applied Power Electronics Conference and Exposition (APEC'04), vol. 3, pp. 1572–1576 (2004)
22. Pappas, G., Rosenfeld, R., Beam, A.: The ARPA/Navy unmanned undersea vehicle program. Unmanned Systems **11**(2), 41–44 (1993)
23. Rosenfeld, R.L., Prokopius, P.R., Meyer, A.P.: Fuel cell power system development for submersibles. In: Proc. of the 1992 Symposium on Autonomous Underwater Vehicle Technology, pp. 184–188 (1992)
24. Smith, R.: Open Dynamics Engine. http://www.ode.org/ (2005)
25. Sourceforgenet: Player/stage/gazebo project page. http://playerstage.sourceforge.net/ (2005)
26. Space and Naval Warfare Systems Command: Joint robotics program, tech database, robotic platforms, unmanned ground vehicles, ATRV-Jr specifications. http://robot.spawar.navy.mil/images/database/Platforms/UGV/doc/atrvjr_tech_2001.pdf (2005)
27. Storvik, M.: Guidance system for automatic approach to a ship. Master's thesis, Norwegian University of Science and Technology (2003)
28. Sunwize Technologies, Inc: Homepage. http://www.sunwize.com/ (2005)
29. Swider-Lyons, K.E., Carlin, R.T., Rosenfeld, R.L., Nowak, R.J.: Technical issues and opportunities for fuel cell development for autonomous underwater vehicles. In: Proceedings of the 2002 Workshop on Autonomous Underwater Vehicles, pp. 61–64 (2002)

30. Wilhelm, A., Pharoah, J., Surgenor, B.: Fuel cell today – fuel cells and mobile robots. http://www.fuelcelltoday.com/FuelCellToday/FCTFiles/FCTArticleFiles/Article_933_FuelCellsandMobileRobots.pdf (2006)
31. Yamamoto, I., Aoki, T., Tsukioka, S., Yoshida, H., Hyakudome, T., Sawa, T., Ishibashi, S., Inada T., Yokoyama, K., Maeda, T., lshiguro, S., Hirayama, H., Hirokawa, K., Hashimoto, A., Hisatome, N., Tani, T.: Fuel cell system of AUV urashima. In: Proc. of OCEANS'04 MTS/IEEE TECHNO-OCEAN'04, 3, 1732–1737 (2004)
32. Zheng, F., Garg, N., Sobti, S., Zhang, C., Joseph, R.E., Krishnamurthy, A., Wang, R.Y.: Considering the energy consumption of mobile storage alternatives. 11th IEEE/ACM International Symposium on Modeling, Analysis and Simulation of Computer Telecommunications Systems, MASCOTS 2003, pp. 36–45, 12–15 October 2003